JACS
JOURNAL OF THE AMERICAN CHEMICAL SOCIETY
Article
pubs.acs.org/JACS

Heck Coupling of Olefins to Mixed Methyl/Thienyl Monolayers on Si(111) Surfaces

Leslie E. O'Leary, Michael J. Rose, Tina X. Ding, Erik Johansson, Bruce S. Brunschwig, and Nathan S. Lewis*

Beckman Institute and Kavli Nanosciences Institute, Division of Chemistry and Chemical Engineering, 210 Noyes Laboratory, California Institute of Technology, Pasadena, California 91125, United States

Supporting Information

ABSTRACT: The Heck reaction has been used to couple olefins to a Si(111) surface that was functionalized with a mixed monolayer comprised of methyl and thienyl groups. The coupling method maintained a conjugated linkage between the surface and the olefinic surface functionality, to allow for facile charge transfer from the silicon surface. While a Si(111) surface terminated only with thienyl groups displayed a surface recombination velocity, S, of 670 ± 190 cm s^{-1}, the mixed CH_3/SC_4H_3–Si(111) surfaces with a coverage of $\theta_{SC_4H_3}$ = 0.15 ± 0.02 displayed a substantially lower value of S = 27 ± 9 cm s^{-1}. Accordingly, CH_3/SC_4H_3–Si(111) surfaces were brominated with *N*-bromosuccinimide, to produce mixed CH_3/SC_4H_2Br–Si(111) surfaces with coverages of θ_{Br-Si} < 0.05. The resulting aryl halide surfaces were activated using $[Pd(PPh_3)_4]$ as a catalyst. After activation, Pd(II) was selectively coordinated by oxidative addition to the surface-bound aryl halide. The olefinic substrates 4-fluorostyrene, vinylferrocene, and protoporphyrin IX dimethyl ester were then coupled (in dimethylformamide at 100 °C) to the Pd-containing functionalized Si surfaces. The porphyrin-modified surface was then metalated with Co, Cu, or Zn. The vinylferrocene-modified Si(111) surface showed a linear dependence of the peak current on scan rate in cyclic voltammetry, indicating that facile electron transfer had been maintained and providing evidence of a robust linkage between the Si surface and the tethered ferrocene. The final Heck-coupled surface exhibited S = 70 cm s^{-1}, indicating that high-quality surfaces could be produced by this multistep synthetic approach for tethering small molecules to silicon photoelectrodes.

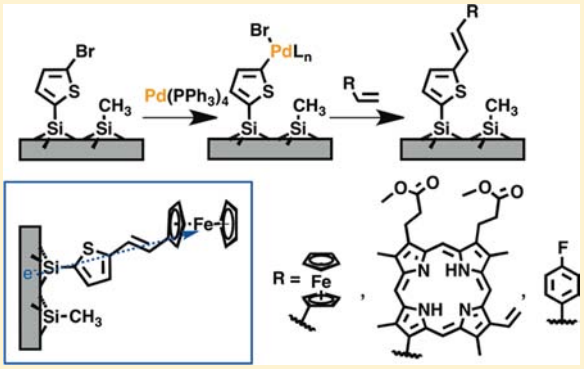

INTRODUCTION

Functionalized silicon surfaces are integral to microelectronics,[1−4] semiconductor photoelectrochemistry and photocatalysis,[5,6] and chemical and biochemical sensor technology.[7−10] The H-terminated Si(111) surface has a low electronic defect-state density and exhibits good interfacial electron-transfer properties in contact with liquid electrolytes that contain suitable one-electron outer-sphere redox couples.[11,12] However, the H-terminated Si(111) surface degrades electrically and chemically within minutes on exposure to air,[13−16] requires high overpotentials to effect the reduction of protons and/or of carbon dioxide at reasonable rates,[17,18] and possesses relatively little chemical selectivity, making it unsuitable for direct use in many device or sensing applications.[9,19−21]

Chemical modification of Si(111), specifically with methyl groups, can produce surfaces that have significantly improved properties relative to H–Si(111) surfaces.[5,16,21,22] For example, methyl-terminated Si(111) surfaces formed by a two-step halogenation/alkylation process or by an anodic functionalization route[23] exhibit chemical passivation properties superior to those of H–Si(111) surfaces and also exhibit facile interfacial charge transfer and low electrical surface-state densities.[11,16] The behavior stems from the complete coverage of atop Si atoms by Si–C bonds as well as from the kinetic stability of Si–C bonds.[24,25] Methyl groups are small enough to terminate every Si(111) atop site on an unreconstructed Si(111) surface. Consistently, CH_3–Si(111) surfaces have been shown to exhibit atomically flat terraces >200 nm in length, as evidenced by scanning tunneling microscopy (STM),[24] polarization-dependent transmission Fourier transform infrared spectroscopy (FTIR),[26] and helium atom scattering (HAS).[25] X-ray photoelectron spectroscopy (XPS),[27,28] soft XPS,[29] scanning Auger microscopy,[30] scanning tunneling spectroscopy,[24] and surface lifetime measurements[16] have all revealed a high degree stability of the CH_3–Si(111) surface toward Si oxidation and a low density of electronic trap states over extended periods of time in air.

Although a methyl group is the only alkyl group that is sterically capable of terminating all of the Si(111) atop sites, in some applications, the presence of chemical functionalities other than methyl groups would be desirable on Si(111) surfaces.[31,32] Si(111) surfaces have been partially terminated by arenes, in a reaction catalyzed by Pd(0) in the presence of base.[33]

Received: March 10, 2013
Published: June 26, 2013

 © 2013 American Chemical Society dx.doi.org/10.1021/ja402495e | J. Am. Chem. Soc. 2013, 135, 10081−10090

Scheme 1

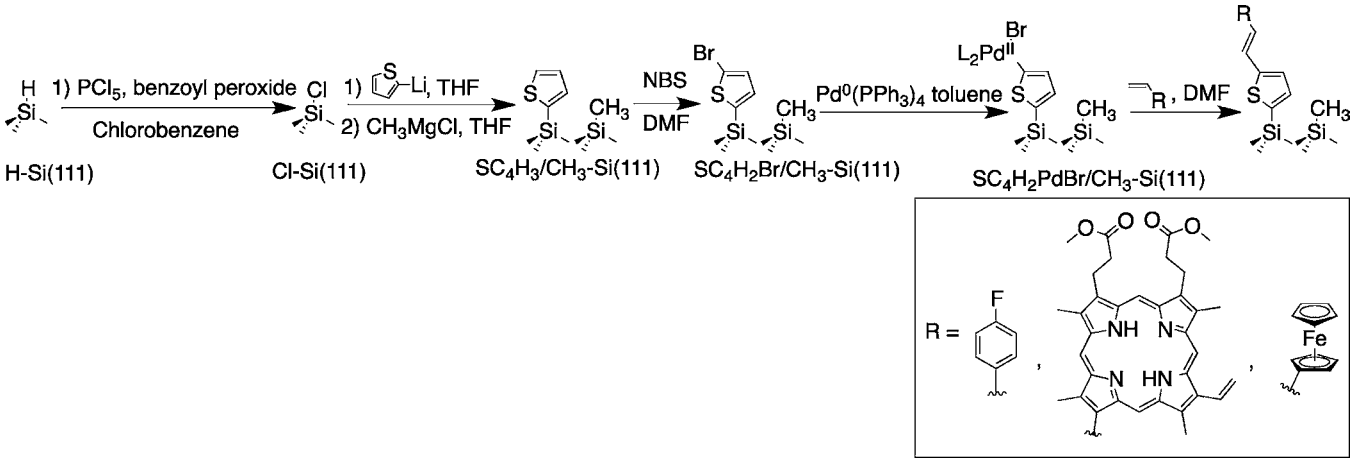

Hydrosilylation has been used to produce a wide variety of Si−C linked monolayers on H-terminated Si surfaces,[34] including ferrocene-functionalized electrodes,[35] layers that can support uniform atomic layer deposition,[36,37] and monolayers that enable a collection of transconduction-based chemical and biochemical sensors.[38] Hydrosilylation is a versatile method for functionalization of Si(111) surfaces, but hydrosilylation is limited to ∼50% coverage of Si atop sites,[39,40] likely leaving adjacent Si−H sites[41] which are susceptible to reactions that produce higher Si oxides.[30]

In more recent work, monolayers of more bulky, synthetically versatile groups have been mixed with $-CH_3$ groups to obtain a higher total overall surface coverage of Si−C bonds.[42] In fact, mixed methyl/allyl monolayers have exhibited close to 100% atop site termination with Si−C bonds, as evidenced by independent FTIR and XPS analysis. The increased overall Si−C termination improved the oxidation resistance in air and decreased the electrical defect state density at such surfaces. Furthermore, the higher surface coverage of Si−C bonds decreased the dependence of the Si band-edge positions on the environment: for example, on the pH of the solution.[43]

To combine the chemical inertness of complete Si−C atop site termination with the desired attribute of having versatile chemical groups on Si surfaces, one promising strategy is to perform secondary functionalization reactions on suitable mixed monolayers.[44,45] The Heck C−C bond-forming reaction[46] offers one potential approach to the preparation of such well-defined, functionalized, mixed monomolecular layers. The thienylated Si(111) surface, which has been synthesized previously and characterized via XPS, Auger spectroscopy, near-edge X-ray absorption fine structure (NEXAFS), and attenuated total reflectance Fourier transform infrared (ATR-FTIR) spectroscopy, can serve as a precursor for Heck chemistry (Scheme 1).[47] Previous work indicates that the Heck coupling chemistry can proceed readily on surfaces, including high-defect-density Si surfaces that have been functionalized by hydrosilylation[48,49] or self-assembled monolayers of thiols on Au surfaces.[50−52] The remaining non-thienyl terminated sites on Si surfaces could in principle be terminated with $Si-CH_3$, to obtain the desired combination of Si−C coverage and chemical functionality. Accordingly, we describe herein the synthesis, reaction chemistry, and electronic properties of mixed CH_3/SC_4H_3 monolayers on Si(111). The aryl bromination, Pd addition, and Heck coupling reactions were monitored by XPS, and the properties of the resulting surfaces were characterized using microwave conductivity decay, grazing-angle attenuated total reflectance infrared (GATR-FTIR) spectroscopy, and electrochemical methods.

EXPERIMENTAL SECTION

A. Materials and Methods. *N*-Bromosuccinimide (NBS) was recrystallized in water, to obtain white crystals. All other chemicals were used as received. H_2O was obtained from a Barnstead Nanopure system, and had a resistivity of ≥18.2 MΩ cm.

Unless specified, double-side-polished, float-zone-grown n-Si samples (Silicon Quest International) had surfaces that were oriented to within ±0.5° of the (111) crystal plane. The samples had a resistivity of 63−77 Ω cm and a thickness of 440 ± 10 μm. Minority-carrier lifetimes were measured using high-purity, double-side-polished n-Si(111) that had a resistivity of 4−8 kΩ cm and bulk minority-carrier lifetimes, τ_{bulk}, of >1−2 ms. Electrochemical data were obtained using single-side-polished, 0.8−1.0 Ω cm resistivity n-Si(111) samples.

1. Oxidation and Removal of Organic Contaminants from Si Surfaces. After Si(111) wafers were cut to the desired size, pieces of Si were rinsed sequentially with water, methanol, acetone, methanol, and then water. The pieces were then dried under a stream of N_2(g). Organic contaminants were removed by cleaning the Si in hot Piranha acid (1:3 30% H_2O_2:18 M H_2SO_4) (*Caution! Piranha reacts violently with organics.*) followed by heating the solution to 90 °C for 10 min. The Si was then rinsed with copious amounts of water and dried (to near dryness) under a stream of N_2(g). The samples were etched (vide infra) immediately following cleaning with the Piranha solution.

2. Anisotropic Etching To Form Atomically Flat H−Si(111). To etch the surface, Si samples were submerged for 18 s in buffered HF(aq) (semiconductor grade, Transene Company, Inc., Danvers, MA). The solution was drained, and any excess HF(aq) was quickly rinsed away with water. The Si samples were then submerged for 9 min into an 11 M NH_4F(aq) solution that had been degassed by bubbling with Ar for >30 min. During submersion, the samples were occasionally agitated to remove bubbles from the surface of the Si. The Si samples were then removed from the NH_4F solution, rinsed with H_2O, and dried under a stream of N_2(g). Within 5 min of etching, the freshly etched Si surfaces were either placed under vacuum or introduced into a N_2(g)-purged container. A fresh buffered HF(aq) solution was used for every Si sample, and the NH_4F(aq) was replaced after ∼1 cm^2 of wafer had been etched in 5 mL of solution.

3. Chlorination of Si(111). H-terminated Si(111) surfaces were chlorinated using a saturated solution of PCl_5 (Alfa Aesar, 99.998% metal basis) in anhydrous chlorobenzene (Sigma Aldrich, 99.8%) with an initiating amount, <1 mg per 5 mL, of benzoyl peroxide (Sigma Aldrich, 97% reagent grade). The reaction solution was generally heated to 90 °C for 45 min, but the temperature and time did not exceed 95 °C and/or 60 min. The solution was then cooled for 5−10 min. The Cl-

dx.doi.org/10.1021/ja402495e | J. Am. Chem. Soc. 2013, 135, 10081−10090

terminated Si(111) samples were rinsed with chlorobenzene, followed by a rinse with anhydrous tetrahydrofuran (THF) (Sigma Aldrich).

4. Methylation and Thiophenylation of Cl–Si(111). The Cl–Si(111) surfaces were alkylated at 50–60 °C for >3 h in a 1.0 M solution in THF of either thienyllithium (Sigma Aldrich) or CH_3MgCl (Sigma Aldrich, diluted from 3.0 M). Mixed CH_3/SC_4H_3–Si(111) surfaces were prepared by submersion of Cl–Si(111) surfaces for 2–30 min in THF solutions of thienyllithium at 50 °C. The samples were rinsed thoroughly with THF and then immersed into a THF solution of CH_3MgCl for >3 h at 60 °C. The composition of the mixed methyl/thienyl monolayer was controlled by varying the time of reaction, t_{rxn}, between the Cl–Si(111) surface and the thienyllithium solution. After completion of both reactions, the Si samples were rinsed thoroughly with THF and removed from the N_2(g)-purged glovebox. Samples were sequentially sonicated for 10 min in THF, methanol, and water and were then dried under a stream of N_2(g).

5. Bromination of Surface-Bound Thiophene. To brominate the Si surfaces, the thiophene-functionalized surfaces (or the CH_3-terminated Si(111) surfaces in control experiments) were exposed for 20 min at room temperature to a solution of 20 mg of *N*-bromosuccinimide/mL of dimethylformamide (DMF). Care was taken to avoid exposing the reaction mixture to light. After reaction, the samples were rinsed thoroughly with DMF and then with THF.

6. Pd Addition and Heck Coupling. To introduce Pd onto Si surfaces, Si(111) samples that had been functionalized with aryl bromides (vide supra) were exposed for 1 h at room temperature to a solution of 5 mg of $Pd(PPh_3)_4$/mL of toluene. The Pd-activated samples were then rinsed thoroughly with toluene, followed by a rinse with DMF. The sample was then submerged into a 0.5–0.8 M solution of a terminal olefin in DMF. The reaction mixture was sealed in a pressure vessel, and the vessel was wrapped in foil to prevent exposure to light and heated to 100 °C for 30 min. The reaction mixture was cooled and then opened to air. The Si sample was rinsed sequentially with water, methanol, acetone, methanol, and water.

B. Characterization and Electrochemistry. *1. FTIR Spectroscopy.* Fourier transform infrared (FTIR) spectra were collected using a Thermo Scientific Nicolet 6700 FT-IR spectrometer that was equipped with a deuterated triglycine sulfate (DTGS) detector and a purified air purge. Attenuated total reflectance (ATR) spectra were recorded using a GATR accessory (Harrick Scientific Products, Inc.), in which samples were pressed against a hemispherical Ge crystal and illuminated at a fixed (65°) angle of incidence. The instrument parameters were set for 4 cm^{-1} resolution. The throughput of the GATR accessory was 11.8% at 2500 cm^{-1}. Prior to acquisition of spectra, the samples were cleaned by rinsing sequentially with water, methanol, acetone, methanol, water, and trichloroethylene. The Ge crystal was cleaned with methyl ethyl ketone. All reported IR spectra represent averages of greater than 3000 consecutive scans.

2. X-ray Photoelectron Spectroscopy. X-ray photoelectron spectroscopy (XPS) data were collected using a Surface Science Instruments M-Probe system.[27] Ejected electrons were collected at an angle of 35° from horizontal, and the sample chamber was maintained at $<5 \times 10^{-9}$ Torr. All XPS energies are reported herein as binding energies in eV. Survey scans from 0 to 1000 eV in binding energy were performed to identify the elements that were present on the surface. High-resolution XPS data were analyzed using the ESCA Data Analysis application (V2.01.01; Service Physics, Bend, OR). The thickness of a monolayer of oxidized Si was calculated as described previously.[53]

The fractional monolayer coverage, Φ_x, of a species of interest, x, was calculated using the fractional substrate–overlayer model (eq 1), where

$$\Phi_{ov} = \left[\frac{\lambda \sin\theta}{a_{ov}}\right]\left(\frac{SF_{Si}}{SF_{ov}}\right)\left(\frac{\rho_{Si}}{\rho_{ov}}\right)\left(\frac{I_{ov}}{I_{Si}}\right) \quad (1)$$

λ is the escape depth of electrons through the overlayer, θ is the angle of electron collection from the surface (35°), a_{ov} is the atomic diameter of the atoms in the overlayer, SF_x is the modified sensitivity factor, ρ_x is the density of species x, and I_x is the collected signal intensity. The value of a_{ov} was calculated from the density of the solid material of concern. Equation 1 holds when $\lambda_{ov} \approx \lambda_{Si}$. The total coverage Φ_{C-Si} of CH_3–Si(111) surfaces was calculated using the intensity of the low binding energy C 1s XP signal of C bonded to Si. θ_{C-Si} of the mixed CH_3/SC_4H_3–Si(111) surfaces was calculated as the sum of the C bonded to Si C 1s XP signal intensity and the S 2s XP signal intensity.

The modified sensitivity factors were calculated as reported previously for the M-probe instrument used in this work (eq 2),[54]

$$SF_m = SF_{scof}\left[\frac{1486 - BE}{1486 - 284}\right]^{S_{exp}} \quad (2)$$

where BE is the binding energy of the analyzed electron, 284 eV is the binding energy of C, and S_{exp} is the sensitivity exponent. For the instrument used in this work, $S_{exp} = 0.6$ for high-resolution scans. Values of SF_x for other elements of interest were as follows: C 1s, 1.00; F 1s, 3.4; Br 3d, 2.84; S 2s, 1.85; Si 2p, 0.90; Pd 3d(5/2), 9.02. The escape depths of photoelectrons were calculated from the empirical equation (3),

$$\lambda = 0.41 a^{1.5} E^{0.5} \quad (3)$$

where E is the photoelectron kinetic energy in eV and a is the diameter of the overlayer atoms. The empirically determined value of $\lambda = 3.5$ nm for Si 2p electrons through long-chain monolayers was used.[55–57] Using these values, $\lambda_{ov} \approx \lambda_{Si}$ was a good approximation for C, S, Br, N, and Pd but was not appropriate for F, Zn, Cu, and Co. Coverages were reported as fractions of a monolayer, θ_x, where $\theta_x = \Gamma_x/\Gamma_{Si(111)}$, with Γ_x being the number density of the species of interest (cm^{-2}) and $\Gamma_{Si(111)}$ the number density of Si atop sites on an unreconstructed Si(111) surface, taken as $\Gamma_{Si(111)} = 7.83 \times 10^{14}$ atoms cm^{-2}.

3. Photoconductivity Decay Measurements. Photoconductivity decay measurements were made using a contactless microwave conductivity apparatus.[16,45] Electron–hole pairs were generated with a 20 ns laser pulse at 905 nm using an OSRAM laser diode with an ETX-10A-93 driver. The lifetime of the excess charge carriers was monitored via the reflected microwave radiation that was detected by a PIN diode. Samples were tested immediately after workup as well as daily for several days after preparation. Between data collections, samples were stored in the dark, in air. The surface recombination velocity stabilized within a few days after preparation of the surface. For measurements taken at various reaction times, t_{rxn} the reaction solutions were drained and the sample was rinsed with THF. Samples were then sealed in a Petri dish and removed from the glovebox, to perform air-free carrier lifetime measurements.

4. Electrochemistry. Si electrodes were formed from ~1.5 cm^2 pieces of Si wafers. After surface functionalization, Ga–In eutectic was scratched into the back of the wafers, to produce ohmic contacts. High-purity Ag paint (SPI supplies) was then used to fix the Si sample to a spool of tinned Cu wire. The wire was strung through a glass tube, and epoxy (Loctite 9460F) was used to protect the tube entry, the wire, and the back and edges of the wafer from the solution. The epoxy was then allowed to cure in a desiccator for >24 h. Electrochemical experiments were performed in an Ar(g)-filled drybox that contained <0.3 ppm of O_2(g). Surface-bound redox species were characterized electrochemically using a Gamry Instruments Reference 600 potentiostat. A three-electrode setup was used, with a Pt-mesh counter electrode, a Ag/$AgNO_3$ nonaqueous reference electrode (calibrated, 0.13 V vs $Fc^{+/0}$), and a functionalized Si working electrode. The electrolyte was 1.0 M $LiClO_4$ (Sigma Aldrich, 99.99% metal basis, battery grade) in CH_3CN (passed over a column of activated Al_2O_3). Data were analyzed using the Gamry Framework version 5.61 software package.

RESULTS

A. FTIR Spectroscopy. Figure 1 shows the GATR-FTIR spectra of two compositionally different mixed CH_3/SC_4H_3–Si(111) surfaces, as well as the spectrum of a [2,2′:5′,2″-terthiophene]-5-Si(111), T_3–Si(111), surface, all obtained vs a

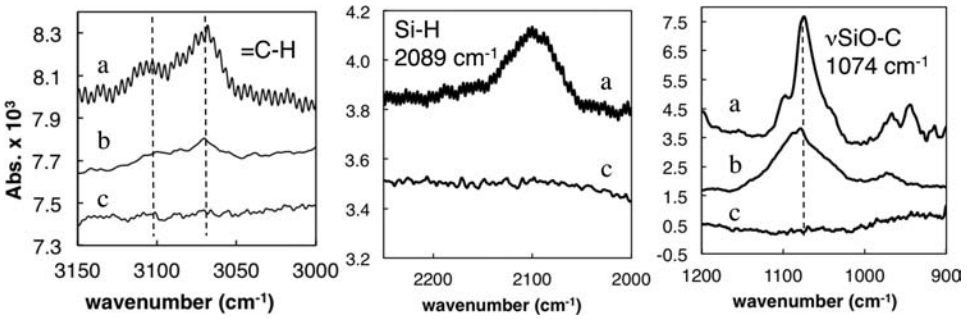

Figure 1. GATR-FTIR spectra of (a) terthiophene (T_3)-functionalized Si(111) synthesized from terthienyllithium in diethyl ether, (b) CH_3/SC_4H_3−Si(111) with $\theta_{SC_4H_3} = 0.54$, and (c) CH_3/SC_4H_3−Si(111) with $\theta_{SC_4H_3} = 0.07$, all referenced vs CH_3−Si(111). Thienyl C(sp^2)−H stretching vibrations at 3067 and 3100 cm^{-1} were observed on mixed CH_3/SC_4H_3−Si(111) surfaces with large $\theta_{SC_4H_3}$ values and were observed yet more prominently on T_3-functionalized Si(111). Surfaces with low θ_{C-Si}, (a) showed Si−H stretching and Si-OC stretching modes, indicative of CH_3OH addition during the workup steps. Surfaces with high θ_{C-Si} and low $\theta_{SC_4H_3}$ did not show evidence of the methoxylation side reaction or exhibit vibrations assignable to H-terminated Si sites.

CH_3−Si(111) background. Vibrational modes characteristic of thiophene were observed in the GATR-FTIR spectra of T_3- and of high coverage, $\theta_{SC_4H_3}$, mixed monolayer CH_3/SC_4H_3−Si(111) samples. The vibrational modes observed at 3060 and 3100 cm^{-1} are assignable to sp^2 C−H stretching modes.

In addition to thiophene-derived modes, vibrational modes were observed at 1074 cm^{-1} (Si−OC stretch) and 2089 cm^{-1} (Si−H stretch). These modes (Figure 1a,b) were observed for surfaces that had a low value of θ_{C-Si} by XPS (vide infra), but these peaks were not observed (Figure 1c) for surfaces that had high θ_{C-Si} values.

B. X-ray Photoelectron Spectroscopy. Figure 2 shows the XP survey spectra of CH_3/SC_4H_3−Si(111) surfaces through a progression of synthetic transformations of the surface functionality. The survey spectrum, as well as the high-resolution spectrum, of the CH_3/SC_4H_3−Si(111) surfaces showed signals

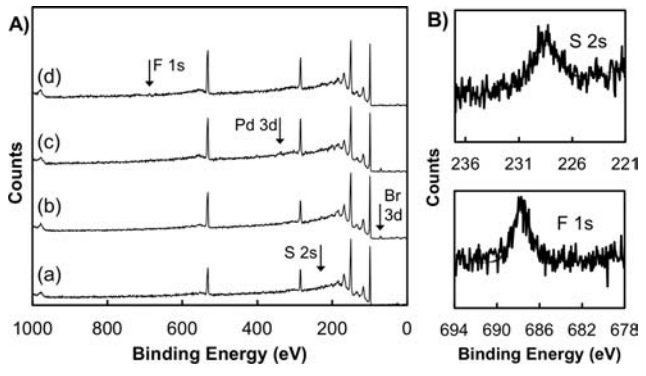

Figure 2. XP survey spectra of a series of CH_3/SC_4H_2X−Si(111) surfaces with $\theta_{SC_4H_3} = 0.24$. Spectra are shown for (a) X = H, (b) X = Br, the NBS-treated CH_3/SC_4H_3−Si(111) surface, (c) X = PdBr, the $Pd(PPh_3)_4$-treated CH_3/SC_4H_2Br−Si(111) surface, and (d) X = FSty, Heck coupling of fluorostyrene to a CH_3/SC_4H_2PdBr−Si(111) surface. A Br 3d signal appeared at ∼70 eV for the CH_3/SC_4H_2Br−Si(111)surface (b). The C 1s signal at 284 eV increased, and a Pd 3d signal appeared for the CH_3/SC_4H_2PdBr−Si(111) surface (c). The C 1s signal remained, a F 1s signal appeared at 689 eV, and the Br 3d signal decreased after the complete Heck coupling of fluorostyrene to the CH_3/SC_4H_2PdBr−Si(111) surface to give the CH_3/SC_4H_2FSty−Si(111) surface (d). High-resolution S 2s and F 1s spectra of the CH_3/SC_4H_2FSty−Si(111) surface. High-resolution Br 3d and Pd 3d spectra are shown in Figures 3 and 4.

that corresponded to the elements Si (∼99, ∼150 eV), C (∼284 eV), S (∼163, ∼229 eV), and O (∼532 eV). Br 3d peaks, at ∼70 eV, were present in spectra that were recorded after exposure of the functionalized Si surfaces to NBS. Pd 3d peaks, at ∼340 eV, were observed after exposure of brominated surfaces to the Pd(0) species. After the Pd-activated functionalized Si surface was heated in a solution of fluorostyrene, the Pd signal was not detected, the Br signal was significantly diminished, and a new F peak at 687 eV was observed.

Values for $\theta_{SC_4H_3}$ were calculated from the high-resolution XPS data for all of the surfaces of interest, using the fractional substrate−overlayer model (section 2B). The reaction of thienyllithium with Cl−Si(111) reached a maximum coverage of $\theta_{SC_4H_3} = 0.55 \pm 0.08$ at 1 h reaction time. Reaction times of 2, 5, or 15 min at 50 °C produced surfaces that had $\theta_{SC_4H_3} = 0.05$, 0.20, and 0.35, respectively.

Subsequent reaction of the thienylated Si(111) surfaces with CH_3MgCl for >3 h at 50 °C enabled the "filling-in" of nonfunctionalized Si surface sites with methyl groups. XPS analysis using the fractional substrate−overlayer model indicated that a high total surface coverage, $\theta_{C-Si} \geq 0.85$, was obtained with $\theta_{SC_4H_3} \leq 0.20$.

Figure 3 shows the high-resolution Br 3d region of the XPS data on a variety of functionalized Si surfaces. Only low levels of Br were observed on the CH_3−Si(111) surface treated with NBS (Figure 3a). In contrast, NBS-exposed CH_3/SC_4H_3−Si(111) surfaces that had low (Figure 3b) and high (Figure 3c) values of $\theta_{SC_4H_3}$ and SC_4H_3−Si(111) surfaces (Figure 3d) exhibited Br signals that were composed of two doublets: a minor doublet that had the same binding energy as Br bound directly to Si (Figure 3e) and a major doublet that was shifted to higher binding energy, at 70.5 eV, indicative of an aryl bromide, as observed previously.[58] The maximum coverage of the thienyl bromide functionality was $\theta_{Br\text{-}SC_4H_2} \leq 0.26 \pm 0.03$. Analysis of the Br−Si signals showed that direct bromination of the Si atop sites proceeded to $\theta_{Br-Si} \leq 0.05$ at CH_3/SC_4H_3− and SC_4H_3−Si(111). For surfaces that had $\theta_{C-Si} \geq 0.5$, control of the Br−Si side reaction was more sensitive to reaction conditions (solvent/NBS purity, exposure to light, reaction temperature) than it was dependent on θ_{C-Si}.

Figure 4 showed the high-resolution Pd 3d XP spectra. The high-resolution XP spectrum of the Pd 3d region observed after

dx.doi.org/10.1021/ja402495e | J. Am. Chem. Soc. 2013, 135, 10081−10090

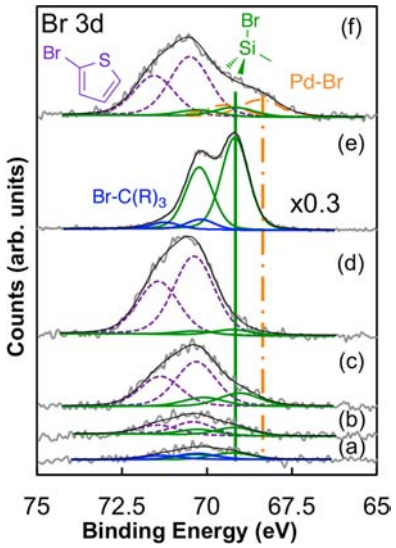

Figure 3. High-resolution Br 3d spectra of (a) CH_3−Si(111), (b) CH_3/SC_4H_3−Si(111) with $\theta_{SC_4H_3}$ = 0.06 and (c) with $\theta_{SC_4H_3}$ = 0.24, (d) SC_4H_3−Si(111), and (e) H−Si(111) all after bromination with NBS. The aryl bromide appeared at a higher binding energy of ∼70.5 eV, in comparison to Br−Si (scaled ×0.3), which exhibited a signal at a binding energy of ∼69.5 eV. With increasing $\theta_{SC_4H_3}$, the amount of aryl bromide increased. Small amounts of another brominated C species were present at brominated H−Si(111) and CH_3−Si(111). (f) After addition of Pd, an electron-rich Br species appeared at a binding energy of 68.3 eV, with approximately the same coverage as Pd(II).

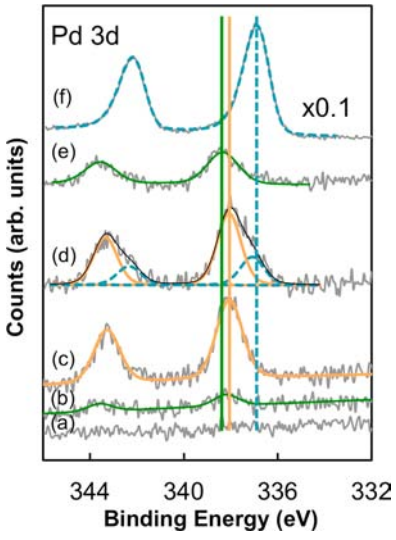

Figure 4. High-resolution Pd 3d XP spectra for exposure of the (a) CH_3/SC_4H_2Br−Si(111) surface to $Pd^{II}(PPh_3)_2Cl_2$, (b) CH_3−Si(111) surface to NBS followed by $Pd(PPh_3)_4$, (c) CH_3/SC_4H_2Br−Si(111) surface to $Pd(PPh_3)_4$, and (d) SC_4H_3−Si(111) surface to $Pd(PPh_3)_4$. Although treatment of the brominated thiophene surface CH_3/SC_4H_2Br−Si(111) with Pd(II), $Pd^{II}(PPh_3)_2Cl_2$ (a), resulted in no detectable addition of Pd, treatment with Pd(0), $Pd(PPh_3)_4$ (c), yielded Pd(II) on the surface. The SC_4H_3−Si(111) surface treated with $Pd(PPh_3)_4$ (d) shows an asymmetric Pd peak indicative of Pd binding in a fashion similar to that observed on H-terminated Si(111) in (f). The addition of $Pd(PPh_3)_4$ to Br−Si(111) (e) terminated at <0.1 monolayer, whereas large, low-binding-energy Pd 3d signals were observed on H-terminated Si(111) surfaces (f).

exposure of surfaces that contained thienyl bromide groups to a solution of $Pd(PPh_3)_4$ (Figure 4c) was consistent with expectations for oxidative addition of a Pd(0) into the aryl bromide bond, yielding a surface-bound Pd(II) species: $\theta_{Pd(II)}$ = 0.12 ± 0.02. The Pd 3d binding energy of 338.2 eV is in accord with a Pd(II) oxidation state.[59] Exposure of surfaces bearing thienyl bromide groups to $Pd^{II}(PPh_3)_2Cl_2$ resulted in no detectable addition of Pd (Figure 4a).

Several Pd(0) sources bound nonspecifically to Si surfaces; therefore, the choice of $Pd(PPh_3)_4$ was crucial to the subsequent Heck chemistry. Exposure of CH_3−Si(111) surfaces, before or after treatment with NBS, to a solution of $Pd(PPh_3)_4$ resulted in $\theta_{Pd(II)}$ < 0.01 (Figure 4b). Exposure of Br−Si(111) to $Pd(PPh_3)_4$ produced spectra consistent with oxidative addition of Pd(II) (Figure 4e), whereas for H−Si(111), the observed Pd binding energies were indicative of Pd(0) deposition (Figure 4f).

After addition of Pd, the Heck reaction was used to effect the covalent attachment of 4-fluorostyrene, protoporphyrin IX, and vinylferrocene to the functionalized Si(111) surfaces. Figure 2 shows the high-resolution XPS data of the F 1s region of a CH_3/$FStySC_4H_2$−Si(111) surface after the coupling reaction had been performed. Table 1 includes a summary of coupling yields for SC_4H_3−Si(111), mixed CH_3/SC_4H_3−Si(111) with $\theta_{SC_4H_3}$ = 0.30, and control surfaces. To provide a model ligand, protoporphyrin IX was coupled to mixed CH_3/SC_4H_2Br−Si(111) surfaces. Cu, Co, and Zn were also successfully coordinated to surface-bound porphyrins without excessive surface oxidation (Figure 5), yielding $\theta_{Cu\text{-}Por}$ = 0.03, $\theta_{Co\text{-}Por}$ = 0.03, and $\theta_{Zn\text{-}Por}$ = 0.09 for surfaces with θ_{porph} = 0.04, 0.04, and 0.09, respectively. The reactions all proceeded to completion, as indicated by the lack of detectable residual Pd, as well as the observation that $\theta_{Pd} \approx \theta_{FSty}$.

C. Surface Recombination Velocity Measurements. Surface carrier lifetimes were measured for CH_3/SC_4H_3−Si(111) surfaces that had a range of $\theta_{SC_4H_3}$ values, for SC_4H_3−Si(111) surfaces and for $CH_3/FStySC_4H_2$−Si(111) surfaces that had been synthesized using Heck coupling. The SC_4H_3−Si(111) surfaces displayed surface recombination velocity values, S, of 670 ± 190 cm s^{-1}. In contrast, CH_3/SC_4H_3−Si(111) surfaces with low $\theta_{SC_4H_3}$ values showed lower S values, with a much lower standard deviation of S, than did the SC_4H_3−Si(111) surfaces. For example, surfaces with $\theta_{SC_4H_3} \leq 0.35$ had S < 100 cm s^{-1} (Figure 6a). As $\theta_{SC_4H_3}$ increased to >0.4, the magnitude and standard deviation of S also increased; however, S remained below the values measured for SC_4H_3−Si(111) surfaces. The S values for Heck-coupled $CH_3/FStySC_4H_2$−Si(111) surfaces were S = 70 ± 10 cm s^{-1} (Figure 6b).

For CH_3−MgCl and SC_4H_3−Li functionalization reactions at Cl−Si(111), air-free photogenerated carrier lifetimes were measured as a function of t_{rxn} (Figure 7). S increased rapidly and then slowly decreased with t_{rxn} for both CH_3- and SC_4H_3-functionalization. After completion of the reaction, t_{rxn} = 600 min, S continued to decrease for SC_4H_3−Si(111) surfaces for days after workup; however, S of CH_3−Si(111) surfaces remained consistent after reaction workup.

D. Electrochemistry of Bound Ferrocene. The reduction and oxidation of a ferrocene, bound to the Si surface via Heck chemistry, was investigated by cyclic voltammetry. In comparison to the formal potential observed for dissolved ferrocenium/ferrocene ($E^{0'}$ = −0.13 vs $Ag/Ag^+(CH_3CN)$), the ferrocene-functionalized Si surfaces exhibited a redox wave at E = 0.05 V vs $Fc^{+/0}$, indicating that the thiophene linker had little effect on the

dx.doi.org/10.1021/ja402495e | J. Am. Chem. Soc. 2013, 135, 10081−10090

Table 1

		before Heck[a]			after Heck[c]		
X−Si(111)	θ_X	$\theta_{Br\text{-}SC_4H_2}$	θ_{Br-Si}	θ_{Pd}[b]	$\theta_{Br\text{-}SC_4H_2}$	θ_{Br-Si}	$\theta_{FSty\text{-}SC_4H_2}$
H−Si(111)	1.0	0[d]	0[d]	>0.5	0[d]	0[d]	*e*
Br−Si(111)	0.42 ± 0.16	0[d]	0.42 ± 0.16	0.06	0[d]	0.04	0.19
CH_3−Si(111)	1.0	0[d]	0.04 ± 0.02	<0.01	0[d]	0.03 ± 0.02	<0.01
CH_3/SC_4H_3−Si(111)	0.30 ± 0.07[f]	0.15 ± 0.03	0.05 ± 0.01	0.12 ± 0.02	0.06 ± 0.02	0.03 ± 0.01	0.11 ± 0.03
SC_4H_3−Si(111)	0.55 ± 0.08	0.26 ± 0.03	0.03 ± 0.02	0.12 ± 0.02	0.11 ± 0.03	0.02 ± 0.02	0.11 ± 0.02

[a]Measured, using XPS, after exposure to NBS in DMF at 23 °C for 20 min, except for the H−Si(111) surface. [b]Measured after exposure to $Pd(PPh_3)_4$ in toluene at 23 °C for 60 min. [c]Measured after reaction with 4-fluorostyrene in DMF at 100 °C for 30 min. [d]Species in question was not present on surface. [e]Not measured. [f]$\theta_{SC_4H_3}$.

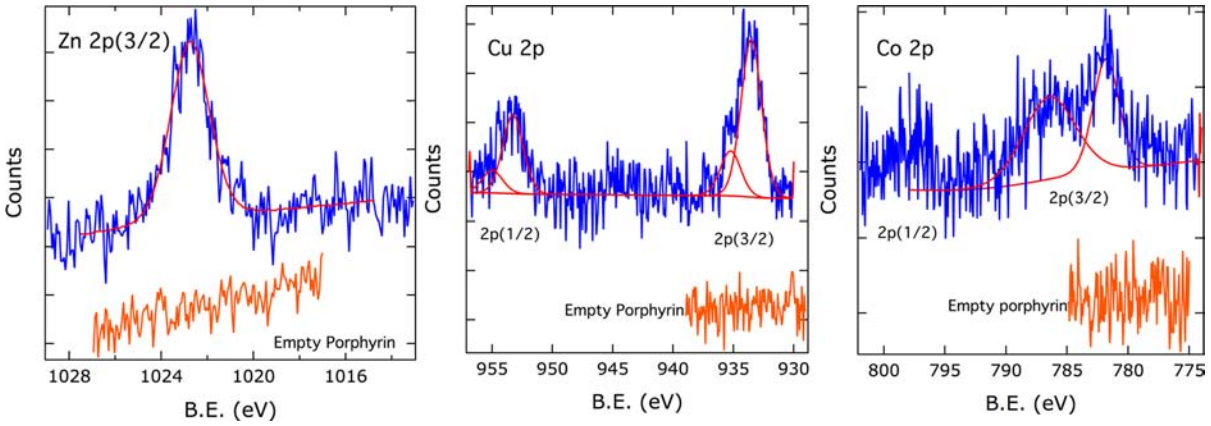

Figure 5. High-resolution XP spectra after metal complexation of surface-bound protoporphyrin IX, yielding θ_M = 0.09 Zn, 0.03 Cu, and 0.03 Co 2p(3/2) with θ_{porph} = 0.09, 0.04, and 0.04, respectively.

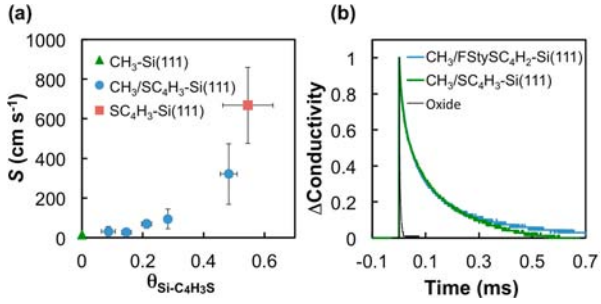

Figure 6. (a) Surface recombination velocity, *S*, as a function of thiophene coverage, $\theta_{SC_4H_3}$. The error bars presented represent ±1 standard deviation. The value of *S* for $\theta_{SC_4H_3}$ < 0.2 was indistinguishable from that for CH_3−Si(111), θ_{CH_3} = 1.0. As $\theta_{SC_4H_3}$ for the CH_3/SC_4H_3−Si(111) surface increased toward that of SC_4H_3−Si(111), *S* increased, as did the standard deviation. SC_4H_3−Si(111) surfaces exhibited large and variable *S* values. (b) Carrier lifetime decay curves for native oxide (black), for CH_3/SC_4H_3−Si(111) with $\theta_{SC_4H_3}$ = 0.15 (green), and for the same surface after the coupling of fluorostyrene via the Heck reaction (blue), indicating little change in *S* values before and after this secondary chemistry was performed.

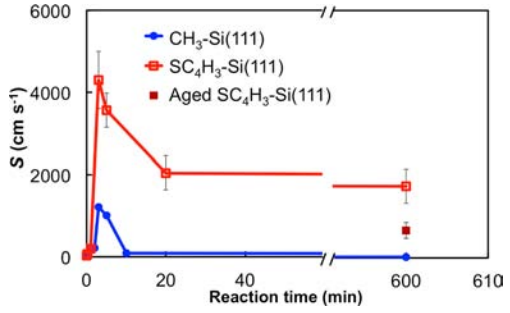

Figure 7. *S* vs t_{rxn} for the reaction of thienyllithium (red open squares) and CH_3MgCl (blue circles) with Cl−Si(111) surfaces as measured in an air-free, contactless microwave conductivity apparatus. Initial Cl−Si(111) surfaces had *S* < 50 cm s^{-1}. The value of *S* rapidly increased at short t_{rxn} and then gradually decreased as the reaction progressed. The value of *S* of surfaces formed by reaction with thienyllithium was much higher than the surfaces formed by reaction with CH_3MgCl, even after completion of the reactions. The value of *S* of SC_4H_3−Si(111) surfaces further decreased after workup (filled red square).

electrochemical potential of the bound ferrocene species (see the Supporting Information). Figure 8 shows the peak cathodic current at a ferrocene-functionalized n-Si(111) electrode vs both the scan rate and the square root of the scan rate in the cyclic voltammetry. The peak cathodic current was linear with the scan rate, indicative of a surface-bound, rather than diffusing, redox-active species.

DISCUSSION

A. Heck Coupling at Si(111) Surfaces. The data indicate that the Heck reaction can provide a robust, facile, and nondestructive method for the coupling of terminal olefins to aryl bromide functionalized Si(111). A small organic molecule (fluorostyrene), a larger heterocycle (protoporphyrin IX), and a redox-active molecule (vinylferrocene) were all successfully coupled to Si(111) surfaces using this approach. With a mixed monolayer CH_3/SC_4H_3−Si(111) surface as the starting point, the aryl groups were brominated with NBS, a common

dx.doi.org/10.1021/ja402495e | J. Am. Chem. Soc. 2013, 135, 10081−10090

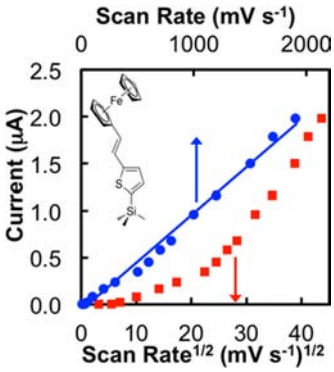

Figure 8. Current ($i_{p,c}$) vs scan rate (blue circles) or vs (scan rate)$^{1/2}$ (red squares) for ferrocene bound to Si(111) via the Heck reaction. The relation was linear with scan rate, not with the square root of the scan rate, confirming that the redox-active species was nondiffusive and thus bound to the surface.

brominating agent, followed by transmetalation using Pd(PPh$_3$)$_4$. Both the arylbromide-functionalized surface and the Pd-functionalized intermediate surface were stable, the Pd-catalyzed C−C bond formation proceeded to completion, and no trace Pd was observed by XPS after the coupling step.

The Heck-based secondary functionalization chemistry of Si(111) surfaces tolerated a broad scope of substrates, yielded clean reactions with no detectable residual Pd by XPS, and resulted in a functionalized Si surface that had a low electronic defect density. Unlike an olefin metathesis method, the Heck reaction does not have "unproductive" turnover events that could be a limiting factor in the attachment of large molecules at a surface.[45,60,61] Furthermore, the Heck chemistry allows for the possibility for complete conjugation from the electrode surface to a surface-bound, redox-active species.

With an observed coverage of $\theta_{SC_4H_3} \geq 0.15$, and considering that the van der Waals radius of the olefinic substrate is less than that of the bound Pd species Si−thienyl−Pd(PPh$_3$)$_n$Br, a generic terminal olefin C=C can thus be coupled to CH$_3$/SC$_4$H$_3$−Si(111) with the maximum $\theta_{C=C} = 0.15$ (see the Supporting Information). This coverage compares favorably to the observed average coverage of $\theta_{C=C} = 0.11 \pm 0.02$, as shown in Table 1. The average coverage of protoporphyrin IX was lower than that of fluorostyrene or vinylferrocene, with $\theta_{porph} = 0.07 \pm 0.03$, likely due to its larger size.

Under our reaction conditions, the terminal olefin coupling step did not appear to proceed through hydrosilylation. Specifically, the coupling of olefins was not observed when CH$_3$/SC$_4$H$_2$Br−Si(111) surfaces were not first exposed to Pd(PPh$_3$)$_4$. Furthermore, the UV-initiated hydrosilylation of fluorostyrene at CH$_3$CH$_2$−Si(111) surfaces, which exhibited $\theta_{CH_3CH_2-Si} = 0.75$ and $S_{CH_3CH_2-Si} = 61$ cm s^{-1}, yielded a mixed CH$_3$CH$_2$/FSty-Si(111) surface that exhibited $S > 650$ cm s^{-1}. Additionally, $\theta_{FSty} \approx \theta_{Br\text{-}SC_4H_2}$(before) − $\theta_{Br\text{-}SC_4H_2}$(after) > θ_{Br-Si}.

B. Formation of Surface-Bound Aryl Bromide. NBS was used to transform surface-bound aryl groups to synthetically versatile aryl halide groups. For CH$_3$/SC$_4$H$_3$−Si(111) mixed monolayers that had $\theta_{SC_4H_3} < 0.2$, a nearly 100% yield of conversion of thiophene to bromothiophene was observed. A maximum of $\theta_{Br\text{-}SC_4H_2} = 0.26 \pm 0.03$ was obtained, on SC$_4$H$_3$−Si(111) surfaces.

NBS was required because direct attachment of bromothiophenes to H−Si(111) by use of (4-bromothienyl)lithium at room temperature and above led to formation of multilayers, and no reaction occurred at −77 °C. NBS has been used as a halogenating agent for H−Si(111),[47,62,63] but treatment of thiophene-functionalized surfaces with recrystallized NBS under rigorously anhydrous conditions, in conjunction with exclusion of light and control of time and temperature (<25 °C), limited the formation of Br−Si surface species to $\theta_{Br-Si} < 0.05$. Specifically, after 20 min of reaction time with NBS, $\theta_{Br\text{-}SC_4H_2}$ did not increase, but θ_{C-Si} decreased and θ_{Br-Si} increased, indicating the onset of side reactions.

C. Pd(II) Intermediate and Addition Parameters. Transmetalation, resulting in a surface-bound Pd(II) species, proceeded readily at Si(111) surfaces that possessed bromothiophene groups. Accordingly, exposure of CH$_3$/SC$_4$H$_2$Br−Si(111) surfaces to a solution of Pd(PPh$_3$)$_4$ yielded a Pd-bound intermediate surface. The XPS data for the BrL$_n$Pd^{II}−SC$_4$H$_2$−Si(111) intermediate surface confirmed the Pd oxidation state as Pd(II), with Pd signals observed at a binding energy of 338.2 eV (Figure 3f). Further evidence of oxidative addition was the observation of a Br XP signal at 68.4 eV (Figure 4c), i.e. at a binding energy close to that of Br$^-$, shifted from the 70.42 eV signal that is associated with Br bonded directly to the thiophene ring (Figure 3d). Toluene, THF, and CH$_2$Cl$_2$ were suitable solvents for the transmetalation. The P XPS signal of the PPh$_3$ ligands was obscured because the dominant P signals overlapped with the core−electron Si binding energies and with the Si phonon loss modes.

The success of the reaction steps depended significantly on the use of pure Pd(PPh$_3$)$_4$ as the Pd source. Other Pd sources, such as Pd(dba)$_2$ and Pd$_2$(dba)$_3$, or even low-purity Pd(PPh$_3$)$_4$, added nonspecifically to the surface or resulted in uncontrolled Pd multilayer formation, even on CH$_3$−Si(111) surfaces.

In contrast to the oxidative addition observed for thienyl bromide functionalized Si surfaces, SC$_4$H$_3$−Si(111) surfaces exhibited nonspecific binding of Pd(II). However, the Pd XP signal shape on such surfaces was distinct from the symmetric Voigt shape that was observed after the addition of Pd to surfaces that had aryl bromide groups (Figure 4c). The asymmetric peak shape was well fitted by two Pd signals, one indicative of oxidative insertion of Pd at Si−H and a second signal indicative of Pd(0) addition. The lower binding energy Pd XP signal, observed at both Pd(PPh$_3$)$_4$-exposed SC$_4$H$_3$−Si(111) (Figure 4c) and H−Si(111) (Figure 4f) surfaces, was shifted by −1.3 eV in binding energy from the main Pd signal. The data are consistent with a process in which Pd addition at SC$_4$H$_3$−Si(111) surfaces proceeded at the H-terminated Si sites in a fashion similar to reaction with the H−Si sites on a pure H−Si(111) surface. The absence of the lower binding energy Pd peak for Pd-treated SC$_4$H$_2$Br−Si(111) or mixed CH$_3$/SC$_4$H$_2$Br−Si(111) surfaces indicated that, in such systems, the addition of Pd did not occur through the H-terminated sites.

D. Electronic Defect Density. The low S values for CH$_3$/SC$_4$H$_3$−Si(111) and for CH$_3$/FStySC$_4$H$_2$-terminated Si(111) surfaces that were synthesized via the Heck coupling process indicated that the synthetic transformations described herein did not result in significant trap state densities on the final functionalized Si surfaces. The surface electronic defect density that was observed before the Heck coupling depended strongly on the coverage and composition of the overlayer on the Si surface. SC$_4$H$_3$−Si(111) surfaces exhibited a low total Si−C coverage of $\theta_{SC_4H_3} = \theta_{C-Si} = 0.55 \pm 0.08$ and showed high, and largely variable, surface recombination velocities, with $S = 670 \pm$

dx.doi.org/10.1021/ja402495e | J. Am. Chem. Soc. 2013, 135, 10081−10090

190 cm s^{-1} (Figure 5). In contrast, mixed CH_3/SC_4H_3−Si(111) surfaces, which exhibited $\theta_{SC_4H_3} < 0.2$ and high $\theta_{C-Si} > 0.85$, showed $S = 27 \pm 9$ cm s^{-1}. The S values of mixed CH_3/SC_4H_3−Si(111) surfaces with $\theta_{SC_4H_3} < 0.2$ and $\theta_{C-Si} \geq 0.85$ were indistinguishable from those of the CH_3−Si(111) surface. The mixed monolayer technique therefore allows utilization of thiophene functionalization for photovoltaic or photoelectrochemical applications, despite the extremely low surface carrier lifetimes of SC_4H_3−Si(111) surfaces.

$$S = \sigma \nu_{th} N_t \quad (4)$$

The effective trap state density, N_t, can be calculated from the surface recombination velocity, S, using eq 4, where $\sigma \approx 10^{-15}$ cm^2 is the trap-state capture cross-section, and $\nu_{th} \approx 10^7$ cm s^{-1} is the thermal velocity of charge carriers.[11] For a surface with $\theta_{SC_4H_3} = 0.1$, i.e. 1 thiophene per 10 surface sites, and having a value of $S = 20$ cm s^{-1}, the effective trap state density is $N_t = 2 \times 10^9$ cm^{-2}, i.e., 1 electronic trap site per ~500000 surface sites.

The chemical nature of the nonfunctionalized Si sites dictates the ability of those sites to act as electronic trap states or to participate in further chemical reactions to produce electronic trap states. A high θ_{C-Si} thus correlated strongly in this work with surfaces that had low values of S.

However, *tert*-butyl-functionalized Si(111) surfaces, with $\theta_{C-Si} = 0.42$, exhibit $S < 100$ cm s^{-1}.[53] The difference between S for the SC_4H_3−Si(111) surface and S for the *tert*-butyl-terminated Si(111) surface, which exhibits a similar θ_{C-Si} value,[53] could arise from differences between functionalization of Si with R−MgX relative to functionalization with R−Li. In small molecules, CH_3−Li is known to break Si−Si bonds,[64−66] and on a surface this process would initially produce dangling Si bonds. However, no change in S was observed for mixed CH_3/SC_4H_3−Si(111) surfaces that were synthesized with CH_3Li rather than with the CH_3−MgCl Grignard reagent.

At very short t_{rxn}, $0 \text{ s} \leq t_{rxn} < 30$ s, in the absence of exposure to air, the mixed Cl/CH_3−Si(111) surfaces and Cl/SC_4H_3−Si(111) surfaces both exhibited low S values (Figure 6). A large electronic trap state density has been observed at Cl−Si(111) surfaces;[67] however, a large field has also been shown to be present at the surface.[68] Because the surface field will separate photogenerated electrons and holes to preclude recombination, the low S value of the Cl−Si(111) surface is therefore expected, despite the large density of electronic trap states on such surfaces.

As the surface functionalization progressed, the value of S increased, consistent with a diminished surface field and incomplete passivation of the electronic trap states. As the reaction progressed, S quickly reached a maximum and then slowly decreased. At completion of the reaction of CH_3MgCl with Cl−Si(111), 100% of the surface atop sites were terminated with Si−C bonds, and the CH_3−Si(111) surface exhibited a very low S. The S of SC_4H_3−Si(111) surfaces did not improve to that of CH_3−Si(111) because of the low filling fraction, $\theta_{C-Si} = 0.55 \pm 0.08$, as well as the presence of residual Cl-terminated sites. Unlike C_2H_5− and *tert*-butyl−Si(111) surfaces with low S, some chlorinated sites remained on the SC_4H_3−Si(111) surfaces, as observed by XPS. The difference between the two types of surfaces is consistent with the observation of β-hydrogen transfer at aliphatic C_2H_5−Si(111) surfaces,[69] whereas similar H atom abstraction is not likely to occur on the aromatic thiophene-functionalized surface. Hence, the Si−Cl functionality, and ill-defined electronic trap sites, remained on SC_4H_3−Si(111) surfaces, likely contributing to the high observed S values.

E. Mixed CH_3/SC_4H_3 Monolayers. In previous work, mixed monolayers were synthesized in one pot because the Grignard reagents that were used in the competitive reaction, CH_2CHCH_2MgCl and CH_3MgCl, had mutually similar reaction rates with the Si surface. The monolayer composition could therefore be controlled by changing the mole ratio of reactants in a single solution.[42,43] A sequential functionalization method was instead necessary to produce mixed CH_3/SC_4H_3−Si(111) surfaces. A solution composition of <1 mol % CH_3Li produced 100% CH_3−Si(111) surfaces, indicating that the significantly higher reaction rates of CH_3Li with Si(111) surfaces precluded reaction of thienyllithium with Cl−Si(111) sites in one pot. Thienylation with thienylmagnesium bromide did not yield any detectable addition of thiophene. Because CH_3MgCl and thienyllithium are not mutually compatible, a two-step reaction sequence was therefore adopted in the work described herein.

The composition of the monolayer ($\theta_{SC_4H_3}$) was readily controlled by limiting the thienyl reaction time to between 2 and 15 min, at 50 °C. The partial thienyl monolayer was then filled to completion by immersion of the Cl/SC_4H_3−Si(111) surface into a solution of CH_3MgCl. Surfaces with $0.05 < \theta_{SC_4H_3} < 0.55 \pm 0.08$ were formed using this approach. Mixed monolayers with a coverage of $\theta_{SC_4H_3} < 0.05$ are likely possible, but due to the broad nature of the S 2s XPS signal, the composition of such monolayers was difficult to quantify reliably.

Figure 1 shows the presence of Si−OC stretching modes, 1074 cm^{-1}, at [2,2′:5′,2″-terthiophen]-5-Si(111), T_3−Si(111), and high-$\theta_{SC_4H_3}$ CH_3/SC_4H_3−Si(111) surfaces. The formation of SiO−C bonds has been ascribed to THF ring opening or to methoxylation of nonfunctionalized sites during the reaction workup steps.[70] To eliminate the possibility of THF ring opening, T_3−Si(111) was synthesized in diethyl ether. However, the T_3−Si(111) surfaces still exhibited the 1074 cm^{-1} Si−OC vibrational mode, indicating that this mode most likely appeared as a result of the addition of methanol during the workup steps. Surfaces with higher total θ_{C-Si} are less susceptible to reaction with methanol, as evidenced by the absence of the 1074 cm^{-1} mode on CH_3/SC_4H_3−Si(111) with $\theta_{SC_4H_3} = 0.07$ and total $\theta_{C-Si} > 0.9$ (Figure 1c).

The presence of Si−H stretching modes, 2100 cm^{-1}, was also observed in the FTIR spectra of low total θ_{C-Si} Si(111) surfaces (Figure 1). Si−H has been observed previously on CH_3CH_2−Si(111), *tert*-butyl−Si(111), and other functionalized Si surfaces.[26,69] Isotopic labeling experiments have shown that, in the presence of an sp^3-β hydride, the hydrogen atom comes from Si sites adjacent to those that form Si−H bonds.[69] In the absence of an sp^3-β hydride, some Si−H sites are apparently still formed, while other non-Si−C-terminated sites remain Si−Cl; therefore, in such systems the H termination presumably occurs through the solvent and/or through a separate mechanism.

CONCLUSIONS

A method for the robust secondary functionalization of Si(111) surfaces has been described that allows for the addition of organic or organometallic molecules or metal-binding ligands, with an average coverage of $\theta = 0.11 \pm 0.02$ and without the formation of electronic trap states at the surface. Formation of a synthetically versatile surface-bound aryl bromide with a coverage of $\theta_{Br\text{-}SC_4H_2} = 0.26 \pm 0.03$ is straightforward using the procedure described

dx.doi.org/10.1021/ja402495e | J. Am. Chem. Soc. 2013, 135, 10081−10090

herein. The Heck reaction proceeded cleanly, and no residual surface-bound Pd was detected by XPS. Utilization of the mixed monolayer technique afforded surfaces having low electronic defect densities (roughly 1 in 500000 sites) and exhibiting S values as low 27 ± 9 cm s^{-1} for CH_3/SC_4H_3–Si(111) with $\theta_{SC_4H_3} < 0.2$ before Heck functionalization and $S = 70$ cm s^{-1} after the coupling reaction. The mixed-monolayer technique minimized residual Si–Cl electronic trap sites and deleterious secondary reactions, such as methoxylation of nonfunctionalized Si atop sites. An analysis of the peak voltammetric current vs scan rate of the surface functionalized with vinylferrocene confirmed that ferrocene had been covalently bound to the surface and that the thiophene linker did not significantly shift the electrochemical potential of the bound redox species or impede electron transfer processes significantly, on the time scale of the voltammetry.

■ ASSOCIATED CONTENT

Supporting Information

Figures and text giving XPS spectra of various Si surfaces, cyclic voltammetry of surface-attached ferrocenes on Si, substrate–overlayer model calculations, and molecular models of functionalized Si surfaces. This material is available free of charge via the Internet at http://pubs.acs.org.

■ AUTHOR INFORMATION

Corresponding Author

*E-mail for N.S.L.: nslewis@caltech.edu.

Notes

The authors declare no competing financial interest.

■ ACKNOWLEDGMENTS

This work was supported by the National Science Foundation (CHE-1214152) and the Molecular Materials Research Center of the Beckman Institute at the California Institute of Technolgy. The Link Foundation Energy fellowship (L.E.O.), the NSF ACC-F (M.J.R., CHE-1042009), and the John and Maria Laffin Trust SURF (T.X.D.) are gratefully acknowledged for graduate, postdoctoral, and undergraduate fellowship support. We acknowledge Dr. Ronald Grimm and Ms. Judith Lattimer for insightful discussions.

■ REFERENCES

(1) Clem, P. G.; Jeon, N. L.; Nuzzo, R. G.; Payne, D. A. *J. Am. Ceram. Soc.* **1997**, *80*, 2821.
(2) Srinivasan, U.; Houston, M. R.; Howe, R. T.; Maboudian, R. *J. Microelectromech. Syst.* **1998**, *7*, 252.
(3) Ashurst, W. R.; Yau, C.; Carraro, C.; Lee, C.; Kluth, G. J.; Howe, R. T.; Maboudian, R. *Sens. Actuators, A* **2001**, *91*, 239.
(4) Ko, H.; Peleshanko, S.; Tsukruk, V. V. *J. Phys. Chem. B* **2004**, *108*, 4385.
(5) Bansal, A.; Lewis, N. S. *J. Phys. Chem. B* **1998**, *102*, 1067.
(6) Lewis, N. S. *J. Electroanal. Chem.* **2001**, *508*, 1.
(7) Lin, V. S. Y.; Motesharei, K.; Dancil, K. P. S.; Sailor, M. J.; Ghadiri, M. R. *Science* **1997**, *278*, 840.
(8) Parce, J. W.; Owicki, J. C.; Kercso, K. M.; Sigal, G. B.; Wada, H. G.; Muir, V. C.; Bousse, L. J.; Ross, K. L.; Sikic, B. I.; McConnell, H. M. *Science* **1989**, *246*, 243.
(9) Strother, T.; Cai, W.; Zhao, X. S.; Hamers, R. J.; Smith, L. M. *J. Am. Chem. Soc.* **2000**, *122*, 1205.
(10) Bent, S. F. *Surf. Sci.* **2002**, *500*, 879.
(11) Yablonovitch, E.; Allara, D. L.; Chang, C. C.; Gmitter, T.; Bright, T. B. *Phys. Rev. Lett.* **1986**, *57*, 249.
(12) Tan, M. X.; Lewis, N. S. *Inorg. Chim. Acta* **1996**, *242*, 311.
(13) Mende, G.; Finster, J.; Flamm, D.; Schulze, D. *Surf. Sci.* **1983**, *128*, 169.
(14) Niwano, M.; Kageyama, J.; Kurita, K.; Kinashi, K.; Takahashi, I.; Miyamoto, N. *J. Appl. Phys.* **1994**, *76*, 2157.
(15) Zhang, X.; Garfunkel, E.; Chabal, Y. J.; Christman, S. B.; Chaban, E. E. *Appl. Phys. Lett.* **2001**, *79*, 4051.
(16) Royea, W. J.; Juang, A.; Lewis, N. S. *Appl. Phys. Lett.* **2000**, *77*, 1988.
(17) Dominey, R. N.; Lewis, N. S.; Bruce, J. A.; Bookbinder, D. C.; Wrighton, M. S. *J. Am. Chem. Soc.* **1982**, *104*, 467.
(18) Boettcher, S. W.; Warren, E. L.; Putnam, M. C.; Santori, E. A.; Turner-Evans, D.; Kelzenberg, M. D.; Walter, M. G.; McKone, J. R.; Brunschwig, B. S.; Atwater, H. A.; Lewis, N. S. *J. Am. Chem. Soc.* **2011**, *133*, 1216.
(19) Wang, X. Y.; Landis, E. C.; Franking, R.; Hamers, R. J. *Acc. Chem. Res.* **2010**, *43*, 1205.
(20) Cai, W.; Peck, J. R.; van der Weide, D. W.; Hamers, R. J. *Biosens. Bioelectron.* **2004**, *19*, 1013.
(21) Hamann, T. W.; Lewis, N. S. *J. Phys. Chem. B* **2006**, *110*, 22291.
(22) Maldonado, S.; Knapp, D.; Lewis, N. S. *J. Am. Chem. Soc.* **2008**, *130*, 3300.
(23) Teyssot, A.; Fellah, S.; Ozanam, F.; Chazalviel, J.-N. *Electrochim. Acta* **2002**, *47*, 2565.
(24) Yu, H. B.; Webb, L. J.; Ries, R. S.; Solares, S. D.; Goddard, W. A.; Heath, J. R.; Lewis, N. S. *J. Phys. Chem. B* **2005**, *109*, 671.
(25) Becker, J. S.; Brown, R. D.; Johansson, E.; Lewis, N. S.; Sibener, S. J. *J. Chem. Phys.* **2010**, 133.
(26) Webb, L. J.; Rivillon, S.; Michalak, D. J.; Chabal, Y. J.; Lewis, N. S. *J. Phys. Chem. B* **2006**, *110*, 7349.
(27) Bansal, A.; Li, X. L.; Lauermann, I.; Lewis, N. S.; Yi, S. I.; Weinberg, W. H. *J. Am. Chem. Soc.* **1996**, *118*, 7225.
(28) Webb, L. J.; Nemanick, E. J.; Biteen, J. S.; Knapp, D. W.; Michalak, D. J.; Traub, M. C.; Chan, A. S. Y.; Brunschwig, B. S.; Lewis, N. S. *J. Phys. Chem. B* **2005**, *109*, 3930.
(29) Hunger, R.; Fritsche, R.; Jaeckel, B.; Jaegermann, W.; Webb, L. J.; Lewis, N. S. *Phys. Rev. B* **2005**, 72.
(30) Webb, L. J.; Michalak, D. J.; Biteen, J. S.; Brunschwig, B. S.; Chan, A. S. Y.; Knapp, D. W.; Meyer, H. M.; Nemanick, E. J.; Traub, M. C.; Lewis, N. S. *J. Phys. Chem. B* **2006**, *110*, 23450.
(31) Chen, R.; Kim, H.; McIntyre, P. C.; Porter, D. W.; Bent, S. F. *Appl. Phys. Lett.* **2005**, 86.
(32) Filler, M. A.; Bent, S. F. *Prog. Surf. Sci.* **2003**, *73*, 1.
(33) Yamanoi, Y.; Sendo, J.; Kobayashi, T.; Maeda, H.; Yabusaki, Y.; Miyachi, M.; Sakamato, R.; Nishihara, H. *J. Am. Chem. Soc.* **2012**, *134*, 20433–20439.
(34) (a) Terry, J.; Linford, M. R.; Wigren, C.; Cao, R. Y.; Pianetta, P.; Chidsey, C. E. D. *J. Appl. Phys.* **1999**, *85*, 213. (b) Linford, M. R.; Chidsey, C. E. D. *J. Am. Chem. Soc.* **1993**, *115*, 12631.
(35) Fabre, B. *Acc. Chem. Res.* **2010**, *43*, 1509.
(36) Li, M.; Dai, M.; Chabal, Y. J. *Langmuir* **2009**, *25*, 1911.
(37) Seitz, O.; Dai, M.; Aguirre-Tostado, F. S.; Wallace, R. M.; Chabal, Y. J. *J. Am. Chem. Soc.* **2009**, *131*, 18159.
(38) Ciampi, S.; Harper, J. B.; Gooding, J. J. *Chem. Soc. Rev.* **2010**, *39*, 2158.
(39) Linford, M. R.; Fenter, P.; Eisenberger, P. M.; Chidsey, C. E. D. *J. Am. Chem. Soc.* **1995**, *117*, 3145.
(40) Sieval, A. B.; van den Hout, B.; Zuilhof, H.; Sudholter, E. J. R. *Langmuir* **2001**, *17*, 2172.
(41) Cicero, R. L.; Chidsey, C. E. D.; Lopinski, G. P.; Wayner, D. D. M.; Wolkow, R. A. *Langmuir* **2002**, *18*, 305.
(42) O'Leary, L. E.; Johansson, E.; Brunschwig, B. S.; Lewis, N. S. *J. Phys. Chem. B* **2010**, *114*, 14298.
(43) Johansson, E.; Boettcher, S. W.; O'Leary, L. E.; Poletayev, A. D.; Maldonado, S.; Brunschwig, B. S.; Lewis, N. S. *J. Phys. Chem. C* **2011**, *115*, 8594.
(44) Juang, A.; Scherman, O. A.; Grubbs, R. H.; Lewis, N. S. *Langmuir* **2001**, *17*, 1321.
(45) Plass, K. E.; Liu, X. L.; Brunschwig, B. S.; Lewis, N. S. *Chem. Mater.* **2008**, *20*, 2228.

(46) Heck, R. F.; Nolley, J. P. *J. Org. Chem.* **1972**, *37*, 2320.
(47) He, J.; Patitsas, S. N.; Preston, K. F.; Wolkow, R. A.; Wayner, D. D. M. *Chem. Phys. Lett.* **1998**, *286*, 508.
(48) Yam, C. M.; Cho, J.; Cai, C. Z. *Langmuir* **2004**, *20*, 1228.
(49) Qua, M.; Zhang, Y.; He, J.; Cao, X.; Zhang, J. *Appl. Surf. Sci.* **2008**, *255*, 2608.
(50) Davis, J. J.; Bagshaw, C. B.; Busuttil, K. L.; Hanyu, Y.; Coleman, K. S. *J. Am. Chem. Soc.* **2006**, *128*, 14135.
(51) Munao, D.; van Erven, J. W. M.; Valvo, M.; Garcia-Tamayo, E.; Kelder, E. M. *J. Power Sources* **2011**, *196*, 6695.
(52) Davis, J. J.; Hanyu, Y. *Nanotechnology* **2010**, 21.
(53) Nemanick, E. J.; Hurley, P. T.; Brunschwig, B. S.; Lewis, N. S. *J. Phys. Chem. B* **2006**, *110*, 14800.
(54) Haber, J. A.; Lauermann, I.; Michalak, D.; Vaid, T. P.; Lewis, N. S. *J. Phys. Chem. B* **2000**, *104*, 9947.
(55) Haber, J. A.; Lewis, N. S. *J. Phys. Chem. B* **2002**, *106*, 3639.
(56) Laibinis, P. E.; Bain, C. D.; Whitesides, G. M. *J. Phys. Chem.* **1991**, *95*, 7017.
(57) Tufts, B. J.; Kumar, A.; Bansal, A.; Lewis, N. S. *J. Phys. Chem.* **1992**, *96*, 4581.
(58) Basu, R.; Kinser, C. R.; Tovar, J. D.; Hersam, M. C. *Chem. Phys.* **2006**, *326*, 144.
(59) Binding energies: $Pd(PPh_3)_4$, 335 eV; $Pd(PPh_3)_2Br_2$, 338 eV. See the NISt X-ray Photoelectron Spectroscopy Database (http://srdata.nist.gov/xps/Default.aspx).
(60) Stewart, I. C.; Douglas, C. J.; Grubbs, R. H. *Org. Lett.* **2008**, *10*, 441.
(61) Stewart, I. C.; Keitz, B. K.; Kuhn, K. M.; Thomas, R. M.; Grubbs, R. H. *J. Am. Chem. Soc.* **2010**, *132*, 8534.
(62) Gansle, P. B.; Gruber, B. C.; Jarvis, J. T.; Slaitas, A.; DeJesus, S. M.; DeJesus, K. *Microchem. J.* **1997**, *55*, 222.
(63) Tamao, K.; Hayashi, T.; Ito, Y. *Bull. Soc. Chim. Fr.* **1995**, *132*, 556.
(64) Still, W. C. *J. Org. Chem.* **1976**, *41*, 3063.
(65) Still, W. C.; Mitra, A. *Tetrahedron Lett.* **1978**, 2659.
(66) Hevesi, L.; Dehon, M.; Crutzen, R.; LazarescuGrigore, A. *J. Org. Chem.* **1997**, *62*, 2011.
(67) Cao, P.; Yu, H.; Heath, J. R. *J. Phys. Chem. B* **2006**, *110*, 23615.
(68) Lopinski, G. P.; Eves, B. J.; Hul'ko, O.; Mark, C.; Patitsas, S. N.; Boukherroub, R.; Ward, T. R. *Phys. Rev. B* **2005**, *71*, 125308.
(69) Johansson, E.; Hurley, P. T.; Brunschwig, B. S.; Lewis, N. S. *J. Phys. Chem. C* **2009**, *113*, 15239.
(70) Amy, S. R.; Michalak, D. J.; Chabal, Y. J.; Wielunski, L.; Hurley, P. T.; Lewis, N. S. *J. Phys. Chem. C* **2007**, *111*, 13053.